CLM-P318

CLM-P318

UKAEA RESEARCH GROUP

Preprint

OBSERVATION OF 'SWITCH-ON' SHOCKS IN A MAGNETISED PLASMA

A D CRAIG
J W M PAUL

CULHAM LABORATORY
Abingdon Berkshire

1972

OBSERVATION OF 'SWITCH-ON' SHOCKS IN A MAGNETISED PLASMA

by

A. D. Craig and J. W. M. Paul

(Submitted for publication in Journal of Plasma Physics)

ABSTRACT

The Charybdis experiment is designed to produce shock waves propagating into a magnetized hydrogen plasma in directions parallel and almost parallel to the initial field and, in particular, the 'switch-on' shock.

An initial plasma ($n_{e_1} \sim 7 \times 10^{20}$ m^{-3}, $T_1 \sim 1.3$ eV) is produced in a pyrex chamber (0.46 m diameter, 1.25 m long) containing an axial magnetic field (B_z up to 0.28 T). A magnetic piston is produced by a fast rising radial discharge between a short central and an annular outer electrode at one end of the chamber. The Lorentz force on the current sheet causes axial propagation, and under certain conditions a curved shock front propagates ahead of the piston.

The Alfvén Mach number of the flow is varied by changing the axial field strength. At high Mach number, where a parallel shock should be gas dynamic, no separated shock is found. At low Mach number, where theory predicts 'switch-on' shock behaviour, a clearly separated curved shock front is found which passes through a point of parallel propagation. Magnetic and electric probe measurements at the point of parallel propagation show the presence of a 'switch-on' shock.

It is suggested that the 'switch-on' and adjacent oblique shocks are matched together by an intermediate wave propagating behind the latter and merging with the former.

UKAEA Research Group,
Culham Laboratory,
Abingdon, Berks.

August 1972

1. INTRODUCTION

In this paper we describe an experimental study of shock waves propagating into a magnetized plasma in directions parallel and almost parallel to the magnetic field. In particular we expand on an earlier report (Paul et al, 1971) of evidence for the existence of the 'switch-on' shock (Kantrowitz and Petschek, 1966).

1.1 Theory

In a magnetized plasma there are three anisotropic wave speeds, slow c_s, intermediate c_i and fast c_f. Slow and fast waves involve changes in density and transverse magnetic field, and, when compressive, can steepen to form a shock. The intermediate wave, on the other hand, simply rotates the transverse magnetic field component without any compression and should not form a shock (Kantrowitz and Petschek, 1966).

For a shock to be stable to perturbations, the change of flow speed, $v_1 \rightarrow v_2$, across the shock (in a frame of reference moving with the shock) must cross only one sound speed (Anderson, 1963). This condition is satisfied for perpendicular and oblique fast shocks for which

$$v_1 > c_{f1}, \; c_{i1}, \; c_{s1} \quad ; \quad c_{f2} > v_2 > c_{i2}, \; c_{s2}$$

Such shocks have been produced in many laboratories, (Paul et al, 1965, 1971), Keilhacker et al (1971), Hintz, (1971), Alikhanov et al (1968), and Robson and Sheffield, (1968)). However for parallel propagation, where a non-magnetic, i.e., gas dynamic, solution exists, the stability condition is not straightforward.

We consider parallel propagation on a one fluid model of

the plasma. The ratio of particle to magnetic pressure $\beta = 4\mu_o nKT/B^2$, (S.I. units) has a critical value $\beta_c = 2/\gamma$ (γ = ratio of specific heats) such that for parallel propagation (Kantrowitz and Petschek (1966)):

(a) $\beta > \beta_c$; non-magnetic $c_f > c_i = c_s$;

(b) $\beta = \beta_c$, $c_f = c_i = c_s$;

(c) $\beta < \beta_c$, magnetic $c_f = c_i > c_s$.

If $\beta_1 > \beta_c$ a non-magnetic shock with $v_1 \rightarrow v_2$ crossing a non-magnetic c_f is possible for all Alfvén Mach numbers

$$M_A = \frac{v_1}{V_A} = v_1 \sqrt{\frac{\mu_o n M_i}{B^2}} \quad .$$

However, if $\beta_1 < \beta_c$ then the values of β_2 and v_2 depend on M_A. For sufficiently high M_A we have $\beta_2 > \beta_c$ and $v_2 > c_{i2}$ so that a non-magnetic shock can exist. But if M_A is decreased, there is a critical value

$$\hat{M}_A = \left(\frac{\gamma+1 - \gamma\beta_1}{\gamma - 1}\right)^{\frac{1}{2}}$$

for which $v_2 = c_{i2}$ and below which a non-magnetic shock cannot exist although $\beta_2 > \beta_c$ because $v_1 \rightarrow v_2$ would have to cross both c_f and c_i.

For the possible range $\beta_c > \beta > 0$, $\hat{M}_A$ has the range

$$1 < \hat{M}_A < \left(\frac{\gamma + 1}{\gamma - 1}\right)^{\frac{1}{2}} = 2 \quad (\text{for } \gamma = {}^5/_3) \cdot$$

In summary a non-magnetic shock solution is always possible for $\beta_1 > 2/\gamma$ but for $\beta_1 < 2/\gamma$ only if $M_A > \hat{M}_A$.

The critical Mach number $\hat{M}_A$ must not be confused with the better-known critical Mach number M_A^* above which $v_2 > a$, where

a is the sound speed (= $(\gamma p/nM_i)^{\frac{1}{2}}$), and viscous effects become important.

We shall now consider what happens for parallel propagation when $\beta_1 < \beta_c$ and $1 < M_A < \hat{M}_A$. Magnetic shock solutions exist for which $v_1 > c_{f1}$ and $c_{f2} > v_2 = c_{i2}$ but the flow and field behind are oblique (i.e. $c_f > c_i > c_s$). The transverse components of B and v are 'switched-on' by the shock. The transverse field component B_{T_2} is given by Murphy (1971)

$$\frac{B_{T_2}}{B_o} = \left\{ (M_A^2 - 1) \left[\gamma + 1 - \gamma\beta_1 - M_A^2(\gamma - 1) \right] \right\}^{\frac{1}{2}}$$

where B_o is the initial field. This function is plotted in Fig. 1 for the case $\beta_i = 0$.

The velocity conditions of the 'switch-on' shock involve marginal stability ($v_1 > c_{f1} > v_2 = c_{i2}$) and this has aroused much theoretical interest.

Chu and Taussig (1967) have attempted to solve the problem using a numerical experiment; a small transverse field perturbation ahead of the shock causes it to repolarize and an Alfvén wave is produced behind the shock. This resulting shock is, however, no longer, strictly speaking, of the switch-on type because of the transverse field component ahead. More recently Woods (1971) has concluded that a switch-on shock is stable if its downstream state is supersonic, i.e. $M_A < M_A^*$. $M_A^* = 1.53$ for $\beta_1 = 0$ and decreases approximately linearly to 1.0 at $\beta_1 = 2/\gamma$ (Murphy (1971)). A simple argument which arrives at the same result as that of Woods, can be seen by considering the

two fluid theory of the low frequency dispersion curves in a magnetized plasma; the intermediate branch asymptotically approaches the normal Alfvén velocity ($v_A \cos \alpha$) at low ω and asymptotically approaches the sound speed a at high ω. From the conservation relations for a switch-on shock $v_2 = v_A \cos \alpha$ where α is the angle between the field and normal in the post-shock region. Thus for $M_A < M_A^*$

$$v_2 = v_A \cos \alpha \geq c_{i2} > a_2$$

and so $v_1 \rightarrow v_2$ only crosses one sound speed and the switch-on shock should be stable. For $M_A > M_A^*$

$$v_2 = v_A \cos \alpha \leq c_{i2} < a_2$$

and so v now crosses both c_f and c_i and the switch-on shock should not be stable.

This result implies that for $M_A^* < M_A < \hat{M}_A$ there is a unique situation where no stable solution to the shock jump equations can exist.

1.2 Shock Tube Theory

These theoretical problems led us to seek an experimental solution to the question of the existence of the switch-on shock. For this we require a driving piston which will launch a shock propagating through a plasma with $\beta_1 < 2/\gamma$, in a direction parallel to a magnetic field with $1 < M_A < \hat{M}_A$. The boundary conditions must allow the required transverse magnetic field and flow velocity behind this shock wave.

In principle these conditions can be satisfied using an annular shock tube with an axial magnetic field (B_z) and highly

ionized initial plasma. A radial current (J_R) flowing between the annular electrodes can switch-on a transverse (azimuthal) magnetic field (B_θ) and the $\underline{J}_R \times \underline{B}_z$ force can switch-on the transverse (azimuthal) velocity (v_θ).

The cylindrical geometry of this system, which is necessary for continuity of transverse flow, gives rise to three complications.

1. The magnetic pressure of the driving piston varies as $1/r^2$ and this can lead to a tilting of the front away from parallel propagation.

2. The azimuthal velocity represents a rotation and hence a $\underline{J}_\theta \times \underline{B}_z$ force is required to balance the centripetal acceleration.

3. The heating produced by the shock will give rise to a diamagnetic effect behind the shock.

All these effects are minimised by having an annular spacing which is very much less than the cylindrical radius.

Kemp and Petschek (1959) have analysed the flow in an annular shock tube under idealized conditions. Radial effects are neglected, i.e., infinite planar geometry; the current is applied as a step function; the plasma conductivity is assumed infinite, and $\beta_1 = 0$. For sufficiently large applied radial current this model predicts a fast gas dynamic shock with $M_A > \hat{M}_A$ followed by, and separated from, a slow expansion wave. This expansion wave which carries all the current is the driving piston and is separated from the insulating end wall by a vacuum region. As the radial current

is reduced, M_A decreases until for $M_A = \hat{M}_A$, $v_2 = c_{i2} = c_{s2}$ and the fast shock cannot separate from the slow expansion wave. For still lower total current, the switch-on shock occurs and current is shared between the shock and the piston. The flow behind the shock is oblique with $v_2 = c_{i2} > c_{s2}$ so separation can occur again. This flow pattern has a characteristic double jump in the transverse magnetic field (B_θ). These results are summarized in Fig. 2 for the two cases of most interest for this paper $M_A = 2.4$ and 1.35.

1.3 Experiments

A narrow annular shock tube in which these conditions are approximately valid is difficult to fill with a highly ionized plasma. Such experiments have been performed with an initial neutral gas and 'switch-on' ionizing shocks observed, (Taussig, (1965) Levine (1968)). In two more recent experiments, switch-on shocks may have been produced in a highly ionized plasma. In the first Watson-Munro et al (1968), have studied the propagation and attenuation of large amplitude Alfven waves in a configuration similar to the annular shock tube. To facilitate pre-ionization a short central end electrode was used instead of the inner cylinder. The central current path then forms a pinch discharge. They demonstrated the steepening of a front involving a jump in B_θ but gave no evidence for parallel propagation or for the separation of piston and shock.

In the second experiment, Kurtmullaev et al (1971) used a conical theta-pinch gun to project plasma along an axial magnetic field into an initial plasma. They observe a steady shock-like

profile of B_θ propagating along the field. The change in B_θ is in rough agreement with predictions for a switch-on shock. In the geometry of the experiment there is no obvious return path for the radial current which must arise on the axis and flow to the wall. There is no evidence concerning the separation of the piston and shock. Whistler precursor oscillations are seen in B_θ and B_r but not B_z and this provides some evidence for parallel propagation.

We chose an experimental approach (Paul et al, 1971) similar to that of Watson-Munro with four main differences:

1. Discharge tube with more than twice the diameter.
2. Insulating outer wall and annular end electrodes so that both outgoing and return current paths are through the plasma. Also no flux shield was present outside the discharge chamber.
3. Different method of forming the initial plasma.
4. Approximately square radial current wave form with a fast rise time of 0.5 μsec (compared with 15 μsec).

We describe the apparatus (section 2) and then the initial plasma conditions (section 3). The piston produces a general flow pattern which is described (section 4) for conditions with $M_A > 2$ where a switch-on shock is neither expected nor found. By changing the conditions we can obtain a local annular region with parallel propagation and $M_A < 2$. We present a description (section 5) of this flow pattern and the resulting switch-on shock. Finally we summarize and discuss (section 6) the results presented.

2. CHARYBDIS APPARATUS

The apparatus is shown schematically in Fig. 3. The main vacuum vessel consists of a pyrex glass cylinder (1.25 m long, 0.46 m diameter) with stainless steel end plates. Hydrogen was used in all the experiments discussed in this paper with filling pressures typically 20 mtorr.

A slow rising axial magnetic field (B_z) of up to 0.28 Tesla is produced by discharging a capacitor bank through a set of six coils. The current is clamped at its peak and the field remains essentially constant throughout the period of the discharge. The field is uniform to within 2 per cent throughout the main volume of the discharge chamber, i.e., from the launch end, at $z = 0$ to $z = 0.9$ m.

An initial plasma is produced by an oscillatory axial current (100 μsec period, 110 kA peak) between the annular electrode at the launch end and the far end plate. The current damps over five half cycles and is zero for $t > 250$ μsec.

The main radial discharge is produced by applying an electric field $E_o \sim 200$ kV/m between a central short cylinder electrode ($\ell = 60$ mm, dia. $\doteq 57$ mm) and the outer annular electrode used for the preheating discharge. The capacitor bank is in halves feeding opposite sides of the apparatus through transmission lines. A two stage pulse shaping circuit gives a first approximation to a square wave with the current rising in 0.5 μsec to a peak $I_p = 185$ kA and remaining approximately constant for 3 μsec. The radial current sheet moves axially under the $\underline{J}_r \times \underline{B}_\theta$ force and

rotates under the $\underline{J}_r \times \underline{B}_z$ force.

Many coaxial shock tube experiments (Heiser, (1964), Keck, (1964)) have experienced ablation of material from the back insulator. This material has provided a low inductance current path which shunts some fraction of the total current away from the propagating front. To reduce this effect we positioned a protective glass plate between the easily ablated PTFE and the plasma.

3. INITIAL PLASMA

We have measured the radial and axial distributions of electron density $n_e(r,z,t)$ and temperature $T_e(r,z,t)$ using double Langmuir probes. The electron temperature derived from the probe characteristics is effectively independent of position having a value $T_e \cong 1.3$ eV at $t = 300$ μsec after the start of the pre-heat discharge. The saturation current from the probe is then assumed proportional to the electron density.

The density is independent of axial position up to within 40 mm of the ends. The absolute value of $\int n_e(z)dz$ and hence n_e at $r = 0$ was measured interferometrically using the 3.39μm line from an He-Ne laser (Ashby et al, (1965)).

The radial density distribution at $z = 0.46$ m and $t = 300$ μsec is shown in Fig. 4 for a filling pressure $p_o = 20$ mtorr hydrogen and $B_{z1} = 0.1$ and 0.2T. The reduction of density near the axis is almost certainly caused by the current flow to the annular electrode; it is pronounced at early times but diffuses away later. A compromise between good uniformity and high electron

density was obtained at t = 300 μsec and this time was chosen for triggering the radial discharge.

No attempt was made to measure the neutral atom density $n_n(r,z,t)$. This parameter is involved because for frequencies below about 1 MHz, such as occur in the main flow, the neutrals are coupled into the plasma by charge exchange collisions. Fortunately the initial plasma is formed in almost the same manner and has almost the same parameters, e.g. current, energy, T_e , $n_e(r,z,t)$ etc., as the initial plasma in the TARANTULA experiment, for which measurements (Paul (1970)) show $n_n \approx 0.1\, n_e$. We use this similarity to provide an estimate of n_n in the CHARYBDIS experiment.

4. HIGH MACH NUMBER FLOW

The first set of experiments were performed with

$$p_o = 20 \text{ mtorr } (H_2), \quad B_{z1} = 0.1T$$

for which the initial conditions of section 3 are

$$n_e = 7.0 \times 10^{20} m^{-3}; \quad T_{e1} = 1.3 \text{ eV}; \quad v_{A1} = 82.5 \text{ km/sec},$$

and the main radial discharge had

$$E_o = 200 \text{ kV/m (+ ve centre)}, \quad I_p = 185 \text{ kA}.$$

The structure of the magnetic fields in the discharge was investigated with magnetic probes. A typical probe had three miniature coils (20 turns of 1.5 mm dia. and good frequency response to 10 MHz) oriented to measure the three components of the field (i.e. B_r, B_θ, B_z) simultaneously and independently. The coils were situated at the tip of a pyrex glass shield of 5 mm outside diameter. Such probes were inserted both radially at z = 46 cm and axially at various radii. The probes could be

tilted at the axial ports in order to reach radial positions intermediate between port positions.

We also measured electric fields; an axially inserted coaxial probe (dia = 1 mm, tip separation = 10 mm) gave E_z and an axially inserted two-prong probe (tip separation = 3.5 mm) gave E_r and E_θ.

4.1 Azimuthal Field

In Fig. 5 we show oscillograms of $B_\theta(t)$ at r = 94 mm for different axial positions. From the timing and the variation of the rise time of B_θ, it is clear that a large amplitude disturbance in B_θ is propagating from the launch end with $v_z \sim 200$ km/sec, and steepening to a width $L \cong 30$ mm as it goes. This velocity corresponds to a Mach number $M_A = 2.4$, i.e. greater than $\hat{M}_A$.

From these oscillograms we can construct profiles of $B_\theta(z)$ for successive times from the start of the main radial discharge as in Fig. 6. The value $B_\theta(0)$ is obtained from the main discharge current as measured by Rogowski coils within the transmission line. Standard deviations are shown on one curve only to avoid confusion.

The measurements show the following:

(a) An average perturbation ratio $R = B_{\theta 2}/B_{z_1}$ of about 1.6.

(b) The steepening described above.

(c) There is only one propagating front (i.e. no evidence of separated shock and piston) and behind this B_θ is roughly constant.

(d) Only ~70 per cent of the discharge current flows in the

propagating front. The rest flows in a 0.1 m sheath on the protective glass. (The soda glass used in this experiment showed appreciable ablation. With the pyrex glass used for the experiments of section 5, ablation was reduced and 90 per cent of the current was in the propagating front).

Steepening of the propagating radial current sheet occurs for all radii. The radial variation in arrival time of the front (measured as the peak of $\dot{B}_\theta(t)$), converted to a spatial profile by assuming constant propagation velocity is plotted in Fig. 7. The small error bars indicate good reproducibility. The radial current sheet is tilted with the outer region trailing. The tilt (α) is relatively small ($\sim 5^o$ - 10^o) for 50 mm $<$ r $<$ 125 mm. The form of this profile can be understood in relation to the axial current flowing into the front from behind within a radius r given by

$$I_z(r) = \frac{2\pi r\, B_\theta(r)}{\mu_o} .$$

Profiles of $B_\theta(r)$ and $I_z(r)$ are plotted in Fig. 8 for a position about 0.2 m behind the mid-radius point of the front. The axial current path involves a diffuse central channel with half value radius about 50 mm but extending out to 120 mm, and a diffuse annular return path with r $>$ 190 mm. This axial current flowing into the radial current front makes the radial dependence of the magnetic pressure much less than $1/r^2$ and hence reduces the tilt. For 20 mm $<$ r $<$ 100 mm $B_\theta/B_{z1} \sim$ 1.4 a constant.

4.2 Relation between Field Components

The radial current front involves changes in the other magnetic field components B_z and B_r as well as B_θ. The gradients in all three components steepen as the front propagates.

Fig. 9 shows the $B_z(r)$ profile at some distance behind the front (corresponding to the $B_\theta(r)$ profile of Fig. 8). The flux from between $r = 60$ and 180 mm goes partially into forming a region of enhanced field within the pinch and is partially thrown out to larger radii. The profile in the pinch region is almost independent of distance behind the front but the region of reduced flux extends to larger radii further behind the front. The radial forces involved in producing this profile are discussed fully in the next sub-section.

For $r > 120$ mm there is first an increase in B_z across the front which precedes the decrease shown in Fig. 9. In this region

(i) B_r and δB_z rise sharply (100 nsec) and simultaneously, and have the correct signs for a fast oblique shock.

(ii) B_θ rises less sharply (200 nsec) and about 100 nsec behind B_r and δB_z. (Measured from peak $\dot{B}$).

(iii) Small amplitude high frequency oscillations on all three components are observed running ahead of the main jumps. This also occurs for $r < 120$ mm.

We shall interpret these results as indicating that at larger radii there is a fast oblique shock with jump components B_R and δB_Z and that this is followed by, but not properly separated

from, a radial current sheet giving rise to the jump in B_θ and further changes in B_R and B_z. This change in B_θ cannot form part of the fast shock and almost certainly corresponds to the driving piston. For $r < 120$ mm there is no evidence of formation of an oblique shock. The B_z increase that should accompany such a shock does not occur; in fact the B_z decreases.

The high frequency oscillations have the characteristics of whistler waves as seen in other oblique shock experiments (Robson and Sheffield (1968)). From the oscillograms of these oscillations as shown in Fig. 10, we see that

(i) $B_\theta \approx B_r \approx 0.5\ \delta B_z$ as would be expected from small tilt angle α.

(ii) B_r and δB_z are in phase while B_θ, out of the initial plane, lags by $\pi/4$.

(iii) The dominant frequency $\omega \sim 2 \times 10^7$ rad/sec is approximately $2\omega_{ci}$ with higher frequencies at lower amplitude further ahead of the main jump.

(iv) The dominant wavelength $\lambda \sim 40$ mm fits the theoretical whistler wavelength (Stringer (1963))

$$\lambda \doteq \frac{2\pi M_A \cos\alpha}{\left(M_A^2 - 1\right)^{\frac{1}{2}}\left(M_A^2 - \cos^2\alpha\right)^{\frac{1}{2}}}\left(\frac{c}{\omega_{pi}}\right)$$

for $\alpha = 20^\circ$, in reasonable agreement with experiment for the radius $r = 95$ mm (Fig. 7).

These whistler waves are more heavily damped than could be expected for classical dissipation.

Parallel shock with $M_A > \hat{M}_A$ should be gas dynamic and, in the idealised geometry of Kemp and Petschek (Fig.2), such shocks should involve no magnetic field changes. It would be expected, however, that in our finite geometry a parallel shock would be accompanied by changes in B_z arising from diamagnetic effects; no such changes were seen. In the regions of near parallel propagation the E_z probe, which would detect any axial pressure gradient in such a shock, gave no signal before the arrival of the magnetic front.

Theoretical calculations (Jukes (1957-58)) of the structure of gas dynamic shocks in our Mach number region, assuming classical viscosity and heat conductivity, predict a thickness of approximately 8 ion-ion collision mean free paths for the post shock gas, i.e., ~ 30 cm for a $M_A = 2.4$ shock propagating into our preheat plasma. Further it should be noted from Fig. 2(a) that the idealised plane geometry theory predicts a maximum separation distance of only ~4 cm on the time scale of the experiment and therefore such a broad shock would not separate or indeed fully form.

4.3 Radial Motion of Plasma behind the Front

Radial momentum balance requires that

$$\rho \frac{v_\theta^2}{r} + J_\theta B_z - J_z B_\theta - \frac{\partial p}{\partial r} = 0$$

where for azimuthal symmetry

$$\mu J_\theta = \frac{\partial B_r}{\partial z} - \frac{\partial B_z}{\partial r} \approx - \frac{\partial B_z}{\partial r}$$

$$\mu J_z = \frac{1}{r} \frac{\partial}{\partial r} (r B_\theta)$$

We consider four aspects of the radial force balance:

(1) In the J_R current front the force $\underline{J}_R \times \underline{B}_\theta$ produces propagation, while $\underline{J}_R \times \underline{B}_z$ produces rotation (v_θ). This rotation will tend to move the plasma radially outward unless an adequate centripetal acceleration is provided by a radial force.

(2) Behind the current front an axial current J_z flows into it at small radii and out at large radii. These currents produce radial forces $\underline{J}_z \times \underline{B}_\theta$ (i) inward (pinch) at small radii, and (ii) outward (unpinch) at large radii. The experimental profile $B_z(r)$ of Fig. 9 shows that these forces do move the plasma. These displacements generate azimuthal currents (J_θ) which tend to oppose the radial motion through $\underline{J}_\theta \times \underline{B}_z$ forces directed inward for $r > 120$ mm and outward for $r < 120$ mm.

(3) Well behind the front for $r < 120$ mm the magnetic field profiles are steady, that is almost independent of z with the inward $\underline{J}_z \times \underline{B}_\theta$ force balancing the other outward forces.

(4) For $r > 120$ mm no such steady state is observed. We conclude that the $\underline{J}_z \times \underline{B}_\theta$ unpinch force and the centripetal acceleration cannot be balanced by the $\underline{J}_\theta \times \underline{B}_z$ and $\partial p/\partial r$ forces and the plasma continues to move outwards.

4.4 Reproducibility

Many of the records obtained showed appreciable varia-

tion from shot to shot as is illustrated by the error bars in Figs. 8 and 9. These variations are reduced by as much as 50% for a higher B_{z_1} of 0.2T. The azimuthal symmetry of the discharge was measured from the time of arrival of the external B_z signal at four orthogonal azimuthal positions. The time of arrival varied by less than 75 nsec (≡ 15 mm) for B_{z_1} = 0.1T and 50 nsec (≡ 10 mm) for B_{z_1} = 0.2T. These differences are attributed to weak instability of the axial pinch discharge. A larger axial field has the expected stabilizing effect.

4.5 Polarity Effects

All the above results are for the case of positive polarity on the centre electrode. Certain general differences were found when the device was run with negative polarity:

(1) The propagation velocity was higher by ~15%.

(2) The central pinch was more concentrated with the total current flowing within $r = 60$ mm.

(3) The front was more tilted, average $\alpha \sim 50^{\circ}$; this is a consequence of the more concentrated pinch which leads to a higher magnetic pressure on the front in the region $r < 120$ mm.

Polarity effects have been found with many other coaxial devices, both annular shock tubes (Keck, (1962); Burkhardt and Lovberg, (1962)), and plasma focus (Peacock et al (1968)): as yet no satisfactory explanation has been given.

4.6 Discussion

The current flow from the electrodes forms a coaxial structure with, (i) a central diffuse pinch extending over about half the radius, which feeds (ii) a tilted radial current front and returns in (iii) an annular region near the wall. There is a radial region between the pinch and current return region in which there is almost zero axial current. The radial current front propagates along the tube under the axial pressure of the B_θ field contained in the coaxial current structure.

In the outer regions $r > 120$ mm, there is evidence that an oblique fast shock tries to form and to separate slightly ahead of the main radial current front but the structures overlap. On simple 1-D theory the magnetic piston should be a slow expansion fan and should not steepen. The observed front on the contrary steepens like a shock but as such would have no piston to drive it. This feature of the front could lead to a mistaken idenfication of the piston as a shock.

In the central region $r < 120$ mm the radial current front cannot be a simple piston because some plasma must flow through it to form the diffuse pinch behind. Again the front steepens like a shock but would have to be a switch-on in order to produce the B_θ field.

Unfortunately we do not have sufficient information (e.g. n_e, T_e) to formulate a satisfactory model of this "piston".

5. LOW MACH NUMBER FLOW

The second set of experiments were performed with

$$p_o = 20 \text{ mtorr } (H_2) \quad ; \quad B_{z1} = 0.2T,$$

for which the initial condition of section 3 are

$$n_{e1} = 8.0 \times 10^{20} m^{-3} \; ; \; T_{e1} = 1.3 \text{ eV} \; ; \; v_{A_1} = 154 \text{ km/sec},$$

and the main radial discharge had

$$E_o = 200 \text{ kV/m (-ve centre)} \; ; \; I_p = 185 \text{ kA}.$$

5.1 Double Current Sheet

The behaviour of the plasma is in general similar but more reproducible and only 10% of the current flows across the back insulator. However there is one marked difference in the structure of the propagating radial current front. In Fig.11 we show records of B_θ, δB_z and B_r for the $r = 50$ mm, $z = 0.6$ m. This pattern is typical for the region 25 mm $< r <$ 70 mm and $0.4 \text{ m} < z < 0.6$ m. The most interesting feature is the double jump in B_θ corresponding to two well separated radial current sheets.

The arrival time of these two sheets is plotted in Fig.12 as a function of axial position (z). Both sheets are propagating ($v_z \sim 200$ km/sec) and over 0.25 m there is a small increase in the separation of the sheets. The axial velocities of the sheets decrease as they propagate and the Mach number $M_A < \hat{M}_A$.

The first current sheet is sharp (150 nsec ≡ 30 mm) and reproducible. It appears to have a constant width, i.e. no steepening and no diffusing. The second current sheet is broader (350 nsec ≡ 70 mm) and so far from reproducible that it is not possible to discuss whether it steepens or diffuses.

The radial variation in arrival time of the first current sheet (from $\dot{B}_\theta$ as previously) is shown in Fig.13 for z = 0.6 m. There is clearly a radius $r = r^* \sim 52$ mm at which we have parallel propagation. As r increases beyond r^* the propagation becomes oblique, the shock jump decreases and becomes broader and for $r \geq 80$ mm there is a single current sheet. The outer region (r > 80 mm) with a single J_r sheet is similar to that at large radii for $M_A > \hat{M}_A$ (section 4).

5.2 Switch-on Shock

The inner region of parallel propagation around $r = r^*$, has $M_A < \hat{M}_A$ and division of the current between two separated current sheets. This immediately suggests the interpretation of the first current sheet as a switch-on shock, and the second as the piston.

The simple planar model of a switch-on shock will not fit our observations because Fig.11 shows a change of B_z as well as B_θ across the first current sheet. However, for the region of parallel and near parallel propagation B_θ rises ~50 nsec (≡ 10 mm) in front of B_z. This change of B_θ has the properties of a shock, e.g. propagation

velocity is faster than fast speed and the profile is steady, and as such can only be a switch-on shock.

At positions adjacent to r^* the propagation is oblique and thus a simple fast shock cannot create the B_θ component; the post shock field of an oblique shock remains in the plane defined by the propagation vector and the pre-shock field (r z plane). We suggest that, in this region, there is, associated with the oblique shock, an intermediate wave which rotates the transverse field of the shock in order to produce a B_θ; this is discussed fully in a later sub-section. An intermediate shock, if such exists, could not create a large B_θ field by rotating the small initial B_R components (from any lack of parallelism of propagation).

We interpret this B_θ rise at $r \sim r^*$ as a switch-on shock. The change of B_z behind it we interpret as a consequence of radial plasma motion arising from the forces discussed in Section 4. This is discussed in more detail in a later section.

5.3 Shock Jump

The magnitude of the switched-on B_θ field at $r = r^*$ can be compared with plane shock theory, (Fig.1). For our preheat plasma conditions $\beta \sim 0.02$, i.e. negligible. There is some uncertainty in the value of M_A. This arises from a 12% variation in the preheat density of Fig.4 and the uncertain neutral density (assumed 10% of n_e). The upper and lower limits in M_A, assuming a density $\rho = 1.1\, n_e m_i$ ±12% is coupled to the flow, are plotted as a function of z in

Fig.14(a). For these values of M_A the magnitude of the switched-on B_θ component is a steep function (Fig.1) of M_A and thus the uncertainty in the measured M_A makes the comparison with theory difficult. Fig.14(b) shows the range of theoretical $B_{\theta 2}$ corresponding to the M_A values of Fig.14(a). The experimental values, also plotted, lie within the theoretical predictions. Theory and experiment are therefore consistent.

5.4 Fast Oblique Shock and Intermediate Wave

We now discuss the relationship of the switch-on shock existing at $r = r^*$ to the fast oblique shocks on either side. In the oblique region the B_θ component cannot arise from a fast wave. The B_θ component is perpendicular to the plane of the preshock field and propagation vector and so can only be produced by an intermediate wave. Although this wave has the appearance of a shock we hesitate to call it such because we have not demonstrated steepening. For this oblique propagation an intermediate wave can rotate the transverse component behind the fast shock to give the required B_θ component.

This intermediate wave is required to maintain continuity of radial current. The switch-on shock which exists at $r = r^*$ generates a radial current J_r and this must flow outwards. It cannot flow in the oblique fast shock which requires a J_θ current only and so it generates the observed intermediate wave.

This intermediate wave merges with the fast shock near the region of parallel propagation to form the switch-on shock. This is in accord with the nature of this shock; it is a degenerate intermediate and fast shock.

At small angles α (i.e. near r*) the small transverse field ($B_z \sin \alpha$) might be expected to act like that in the stability analysis of Chu and Taussig (1967). They found that a transverse field perturbation changed the switch-on shock structure into an oblique shock followed by an intermediate wave. This is what we propose happens in our experiment.

In Fig. 15 we illustrate the above model using discontinuous transitions spatially close together so that they have the same angle α. The coordinates x, y, θ are related to r,z,θ as shown. From the jump condition across the fast shock and the rotation in the intermediate wave we have (Kantrowitz and Petschek (1966))

$$B_{x1} = B_{x2} = B_{x3}$$

$$B_{y2} > B_{y1} \quad \text{- determined by jump equations}$$

$$(B^2_{y3} + B^2_{\theta 3})^{\frac{1}{2}} = B_{y2} \quad \text{- rotation of transverse field component}$$

$$v_{x2} < v_{x1} \ , \ v_{y2} > v_{y1} \quad \text{- determined by jump equations}$$

$$v_{x3} = v_{x2}$$

and the change in the transverse velocity component through the intermediate wave is given by

$$\Delta \underline{v} = \frac{\Delta \underline{B}}{(\mu_o \rho_2)^{\frac{1}{2}}}$$

where $\Delta\underline{B}$ is the change in transverse field through the intermediate wave. The amplitude of $\left(v_y^2 + v_\theta^2\right)^{\frac{1}{2}}$ does not remain constant in the intermediate wave (except at the switch-on point) and the angle of rotation of the transverse velocity vector is different from that of the transverse magnetic field vector.

Fig.16(a), (b) and (c) shows theoretical curves of p_3, $v_{\theta 3}$ and ρ_3 versus α for the case of an $M_A = 1.3$ shock (at the normal point) propagating into a plasma containing a 0.2T field and having $v_A = 154$ km/sec; we assume that $B_R = 0$ behind the intermediate wave. Fig.16(d) shows the relative velocity of the oblique shock and the intermediate wave (i.e. $v_{x2} - B_{x_2}/(\mu\rho_2)^{\frac{1}{2}}$) plotted as a function of α. This shows that on the time scale of the experiment the separation distance between the shock and intermediate wave should be less than the shock thickness; no indication of separate structures was seen experimentally.

5.5 Conditions behind the Shock

The radial variation of B_θ, B_z and B_r about 60 mm behind the shock ($z = 0.6$m) are shown in Fig.17. The axial variations can be seen from the oscillograms of Fig.11 with $z = v_z t$. At $r = r^* = 52$ mm there is maximum switched on B_θ, maximum reduction of B_z and 'breakaway' point for B_r.

We now consider the radial forces existing behind the

shock/intermediate wave discussed in the previous section. A rotation exists across the complete radial extent which requires a centripetal acceleration v_θ^2/r. For $r < 50$ mm the inward pinch-force ($J_z B_\theta$) provides some inward acceleration. For $r > 50$ mm no force can provide the centripetal acceleration and thus plasma and associated magnetic field must move outwards producing the observed changes in B_r and B_z and generating an inward $J_\theta B_z$ force. The finite B_r in Fig. 17 indicates that no steady state pressure balance is achieved.

Behind the piston the magnetic field profiles are similar to those found for the high M_A flow (section 4).

5.6 Shock Structure

Bickerton et al (1971) have computed theoretical switch-on shock structures, using a two fluid approximation and collisional transport coefficients.

Assumptions made are:-

(i) Bulk viscosity is classical; here we are concerned with sub-critical shocks ($M_A^* = 1.53$ for $\beta_1 = 0$) i.e., no viscous sub-shock forms and the structure is not strongly dependent on viscosity.

(ii) T_e and T_i are tied together; in practice most of the heating will go to the electrons but some degree of thermalization would be expected with such broad structures.

(iii) Shear viscosity is neglected.

(iv) Resistivity varies classically within the shock, i.e. $\eta \propto T_e^{-\frac{3}{2}}$, but may be enhanced by some constant factor.

In Fig. 18 computed magnetic structures ($M_A = 1.3$) are compared with the experimental structure from Fig. 11. Computed structures are shown for cases where the pre-shock resistivity is five times and twenty times the classical value. In Fig. 18(a) the final field jump is preceded by a series of large amplitude whistler oscillations.

If the resistivity is sufficiently low that, in order to produce the necessary dissipation, steepening occurs to the degree where dispersive effects become important, shorter wavelength components will propagate ahead as whistler oscillations. Increased resistivity broadens the shock and therefore reduces these dispersive effects as in Fig. 18(b).

The theoretical structure with $\eta \sim 20\ \eta_{class}$ agrees well with the experimental structure. It is clear that some non-classical process is occurring within the shock and is providing the necessary dissipation without the shock steepening to the degree where dispersive effects are important.

The current density within the shock is obtained directly from the unintegrated $\dot{B}_\theta$ signal

$$J_r = \frac{1}{\mu V_s} \frac{\partial B_\theta}{\partial t} \quad .$$

Typically we find $J_{max} \sim 4.2 \times 10^6$ A/m^2 corresponding to a peak electron drift velocity $v_d (= J_{max}/n_e e) \sim 2.8 \times 10^4$ m/sec. The

plasma sound speed $a = (2\gamma\kappa T_e/m_i)^{\frac{1}{2}}$ at this position is $\sim 3 \times 10^4$ m/sec. The conditions for the onset of the ion acoustic instability (Stringer, (1964)) are $v_d > a$ and $T_e > T_i$. We expect $T_e > T_i$ within the shock because the energy equipartition time between electrons and ions for typical shock conditions ($n_i = 9 \times 10^{20}$ m^{-3}, $T_e = 6 \times 10^4$ °K) is ~ 1 μsec, (Spitzer, (1965). It is possible therefore that ion wave instability is giving rise to the non-classical dissipation within this shock as in other shocks (Paul et al (1971)).

5.7 Electric Field Measurements

An investigation of the electric fields within and behind the shock was made using axially inserted probes. The shot to shot reproducibility on all three components was poor; therefore, rather than attempting any detailed quantitative analysis, we merely demonstrate a general consistency with the model proposed earlier. Fig.19 shows typical oscillograms along with $\dot{B}_\theta$ signals taken with an adjacent magnetic probe.

The electric field within a switch-on shock can be derived from the generalized Ohms law, with electron inertia neglected, i.e.,

$$\underline{E} + \underline{v} \times \underline{B} + \frac{1}{en_i} (\nabla p_e - \underline{J} \times \underline{B}) - \eta \underline{J} = 0.$$

Assuming a plane geometry switch-on shock for simplicity but using cylindrical notation (i.e., $J_\theta = v_r = B_r = 0$), we have

$$E_z = \frac{1}{en_e}\left(J_r B_\theta - \frac{\partial p_e}{\partial z}\right)$$

$$E_\theta = \frac{1}{en_e} J_r B_z$$

$$E_r = \eta J_r - v_\theta B_z + v_z B_\theta \ .$$

Typical parameters at the peak J_r position within the shock, obtained experimentally, are

$$J_r = 4.2 \times 10^6 \ A/m^2 ; \quad B_\theta = 0.08 \ T , \quad B_z = 0.18 \ T$$

and from the theoretical structure of Fig.18(b)

$$n_e = 9 \times 10^{20} \ m^{-3}, \quad T_e = 6 \times 10^4 \ ^\circ K,$$

$$\frac{\partial n_e}{\partial z} = 5 \times 10^{22} \ m^{-4}, \ \frac{\partial T_e}{\partial z} = 5 \times 10^6 \ ^\circ K \ m^{-1} \ .$$

From these the terms involved in the E_z and the E_θ components are therefore

$$\frac{J_r B_\theta}{n_e e} = 2.33 \times 10^3 \ V/m, \quad \frac{1}{n_e e} \frac{\partial p_e}{\partial z} = - 7.2 \times 10^2 \ V/m,$$

$$\frac{J_r B_z}{en_e} = 5.2 \times 10^3 \ V/m \ .$$

Behind our switch-on shock ($M_A \sim 1.2$) the jump equations give the following parameters

$$v_z = 5.4 \times 10^4 \ m/sec, \ v_\theta = 1.07 \times 10^5 \ m/sec, \ B_\theta = 0.17 \ T$$

and experimentally behind the shock $B_z = 0.17 \ T$ ($<0.2 \ T$ due to radial motion). The terms involved in E_r behind the shock are therefore

$$v_z B_\theta = 9.2 \times 10^3 \ V/m, \ v_\theta B_z = 1.28 \times 10^4 \ V/m.$$

A comparison of experimental (from Fig. 19) and theoretical

(derived as above) E field components is contained in the table below.

	Experiment	Theory	Position
E_z	3.0×10^3 V/m	3.0×10^3 V/m	Peak J_r
E_θ	4.8×10^3 V/m	5.2×10^3 V/m	Peak J_r
E_r	2.0×10^4 V/m	2.2×10^4 V/m	Behind shock

The agreement is in each case good. The E_z agreement suggests that the theoretical pressure gradient is indeed present within the shock. The E_r agreement suggests that the theoretical v_θ component is 'switched-on' behind the shock.

In plane geometry E_z and E_θ should drop to zero behind the shock; our geometry is however not plane and other terms in the generalised Ohms law would be expected to contribute in this region e.g. $v_r B_\theta$, $v_\theta B_r$ etc. It is reasonable therefore that, experimentally, E_z and E_θ do not go to zero behind the shock.

5.8 Scaling

A small variation in M_A occurred due to the decrease of the shock velocity with z (Fig. 12). The variation of the jump in B_θ across the shock with M_A over this region has been discussed earlier (5.3). In principle the Mach number could be changed over a much wider range by varying B_{z_1}.

Increasing B_{z_1} to 0.25 T had little effect on the structure of the shock apart from slightly improving the reproducibility. The shock velocity however increased by

an amount which produced approximately the same M_A as in the 0.2 T case discussed earlier.

On decreasing B_{z1} the magnetic structure became less reproducible and for $B_{z1} < 0.17$ T no separated shock-piston structure could be identified. It is possible that the poorer reproducibility is a consequence of the reduced stabilizing field in the focus. It is also perhaps significant that no switch-on shocks could be obtained with $M_A > M_A^*$. ($M_A^* = 1.53$ for $\beta_1 = 0$ (Murphy, (1971)). This may be related to the stability argument discussed in section 1 (Woods, (1971)).

5.9 Discussion

Under certain conditions a curved shock front has been produced which is clearly separated from its driving piston and which contains a point of parallel propagation. The Mach number at this point shows the shock to be in the switch-on regime and indeed a transverse field component in the θ direction is produced behind the shock, the magnitude of which agrees with theory. In order that the flow parameters behind the adjacent oblique parts of the shock can match up with the B_θ and v_θ behind the parallel propagation point we suggest that an intermediate wave follows behind the oblique shock and rotates the transverse velocity and field components to give the necessary B_θ and v_θ. The time scale and structure widths are such that experimentally one would not expect to see a separation of the shock and intermediate wave. Close to the point of parallel propagation the conservation

equations across the shock-intermediate wave pair are essentially the same as those across a pure switch-on shock.

Behind the intermediate wave the heating and rotational forces cause outward radial plasma motion.

Electric probe results are consistent with shock theory; E_z values suggest that the correct degree of compression and heating occurs within the shock; E_r values suggest that the correct azimuthal velocity is switched-on behind the shock.

We have thus demonstrated experimentally that a switch-on shock can exist. The concept of a switch-on shock is perhaps not very realistic in that any infinitesimal angle $\delta\alpha$ away from parallel propagation makes the shock strictly speaking oblique and defines the polarization of the post-shock transverse field. An intermediate wave must then rotate this transverse field into the appropriate direction defined by the boundary conditions behind the shock. It is perhaps more realistic to consider a switch-on shock to be the oblique shock-intermediate wave combination existing for a range of shock angles close to normal.

6. SUMMARY

We have launched large amplitude transverse field disturbances propagating parallel and near parallel to the longitudinal magnetic field of a well diagnosed initial plasma. All three components of magnetic and electric fields have been measured as a function of time and space. Although

reproducibility is not as good as in comparative perpendicular shock experiments (Paul et al (1965)), we have obtained more detailed and more extensive results than previously published for parallel propagation.

For $M_A < \hat{M}_A$ theory predicts a switch-on shock for parallel propagation. We observe a well separated, curved shock front with a local region of parallel propagation. In this region the shock has the characteristics of the expected switch-on shock but is appreciably modified by the effects of cylindrical geometry. The curvature of the shock front requires that the switch-on shock merges into a fast oblique shock. We propose a model for this process which involves an intermediate wave and emphasizes the degenerate fast/intermediate nature of the switch-on shock.

For $M_A > \hat{M}_A$ theory predicts that, for parallel propagation the switch-on solution is replaced by a gas-dynamic solution. We observe that the above switch-on shock does not occur for $M_A > M_A^* < \hat{M}_A$, but there is no evidence of a gas dynamic shock either.

ACKNOWLEDGEMENTS

The authors wish to acknowledge the contribution of Mr. L. S. Holmes in the design and construction of the apparatus.

We are grateful to Dr. R. V. W. Murphy for many useful discussions and to Dr. R. J. Bickerton for his encouragement

and support.

Thanks are also due to Mr. P. Hedley for his technical assistance.

REFERENCES

ALIKHANOV, S.G. et al. Third International Conference on Plasma Physics & Controlled Nuclear Fusion, Novosibirsk (1968) Paper CN-24/A 1 .

ANDERSON, J.E. 'M H D Shock Waves' M I T (1963).

ASHBY, D.E.T.F. et al. J. Appl. Phys., 36, 29 (1965).

BICKERTON, R.J. et al. J. Plasma Physics, 5, 177 (1971).

BURKHARDT, L.C. and LOVBERG, R.C. Phys. Fluids, 5, 341 (1962).

CHU, C.K. and TAUSSIG, R.T. Phys. Fluids, 10, 249 (1967).

HEISER, W.H. Phys. Fluids, 7, 143 (1964).

HINTZ, E. Fourth International Conference on Plasma Physics and Controlled Nuclear Fusion, Madison (1971) Paper CN-28/J-11.

JUKES, J.D. J. Fluid Mech., 3, 275 (1957-58).

KANTROWITZ, A. and PETSCHEK, H.E. In 'Plasma Physics in Theory and Application', Kunkel, W.B. ed. (McGraw-Hill Book Company, Inc., N.Y. 1966).

KECK, J.C. Phys. Fluids, 5, 630 (1962).

KECK, J.C. Phys. Fluids (Suppl), 7, 143 (1964).

KEILHACKER, M. et al, Fourth International Conference on Plasma Physics and Controlled Nuclear Fusion, Madison (1971) Proceedings. IAEA, Vienna, 1971. Vol.3, pp. 265-276.

KEMP, J. H. and PETSCHEK, H. E. Phys. Fluids 2, 599 (1959)

KURTMULLAEV, R. Kh. et al, Soviet Physics JETP, 33, 216 (1971).

LEVINE, L.S. Phys. Fluids, 11, 1479 (1968).

MURPHY, R.V.W. 'Problems in Magnetohydrodynamics' D.Phil. Thesis, 58 (University of Oxford 1971).

PAUL, J. W. M. et al., Nature 208 133 (1965).

PAUL, J. W. M. 'Physics of Hot Plasmas', Oliver and Boyd, (1970) ed. Rye, B. J. and Taylor, J. C., 302.

PAUL, J. W. M. et al. Fourth International Conference on Plasma Physics and Controlled Nuclear Fusion, Madison, (1971). Proceedings. IAEA, Vienna, 1971. Vol. 3, pp. 251-263.

PEACOCK, N. J. et al, Third International Conference on Plasma Physics and Controlled Nuclear Fusion, Novosibirsk (1968). Proceedings. IAEA, Vienna, 1969. Vol. 2, pp. 51-65.

ROBSON, A. E. and SHEFFIELD, J. Third International Conference on Plasma Physics and Controlled Nuclear Fusion, Novosibirsk, (1968). Proceedings. I.A.E.A., Vienna, 1969. Vol.1, pp. 119-128.

SPITZER, L. Jr., 'Physics of Fully Ionized Gases' Interscience (1965), 135.

STRINGER, T. E. Plasma Physics (J. of Nuclear Energy Pt.C) 5, 89 (1963).

STRINGER, T. E. Plasma Physics (J. of Nuclear Energy Pt.C) 6, 267 (1964).

TAUSSIG, R. T. Phys. Fluids, 9, 421 (1965).

WATSON-MUNRO, C. N. et al., Third International Conference on Plasma Physics and Controlled Nuclear Fusion, Novosibirsk, (1968). Proceedings. IAEA, Vienna, 1969, Vol.2, pp. 195-207.

WOODS, L. C., J. Plasma Physics, 6, 615 (1971).

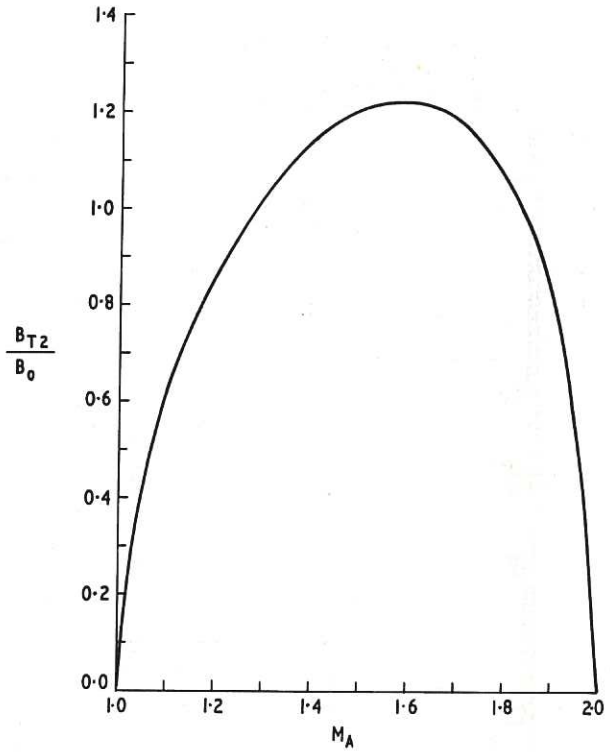

Fig.1 Switched-on transverse field (B_{T_2}) as a function of Mach Number (M_A) ($\beta_1 = 0$, $\gamma = \frac{5}{3}$).

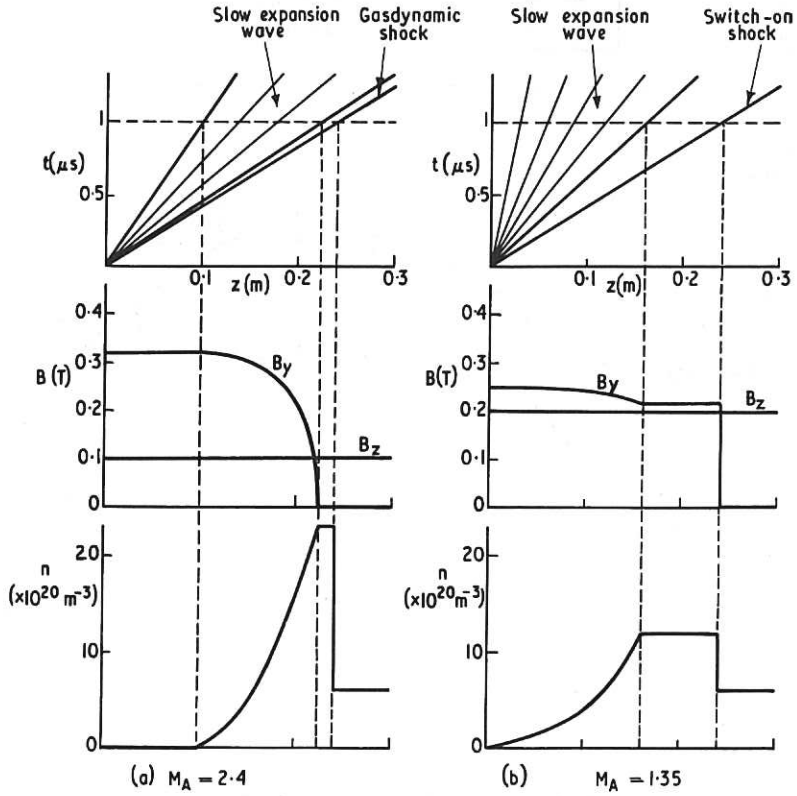

Fig.2 Idealized flow patterns in an annular shock tube (Kemp and Petschek (1959)).

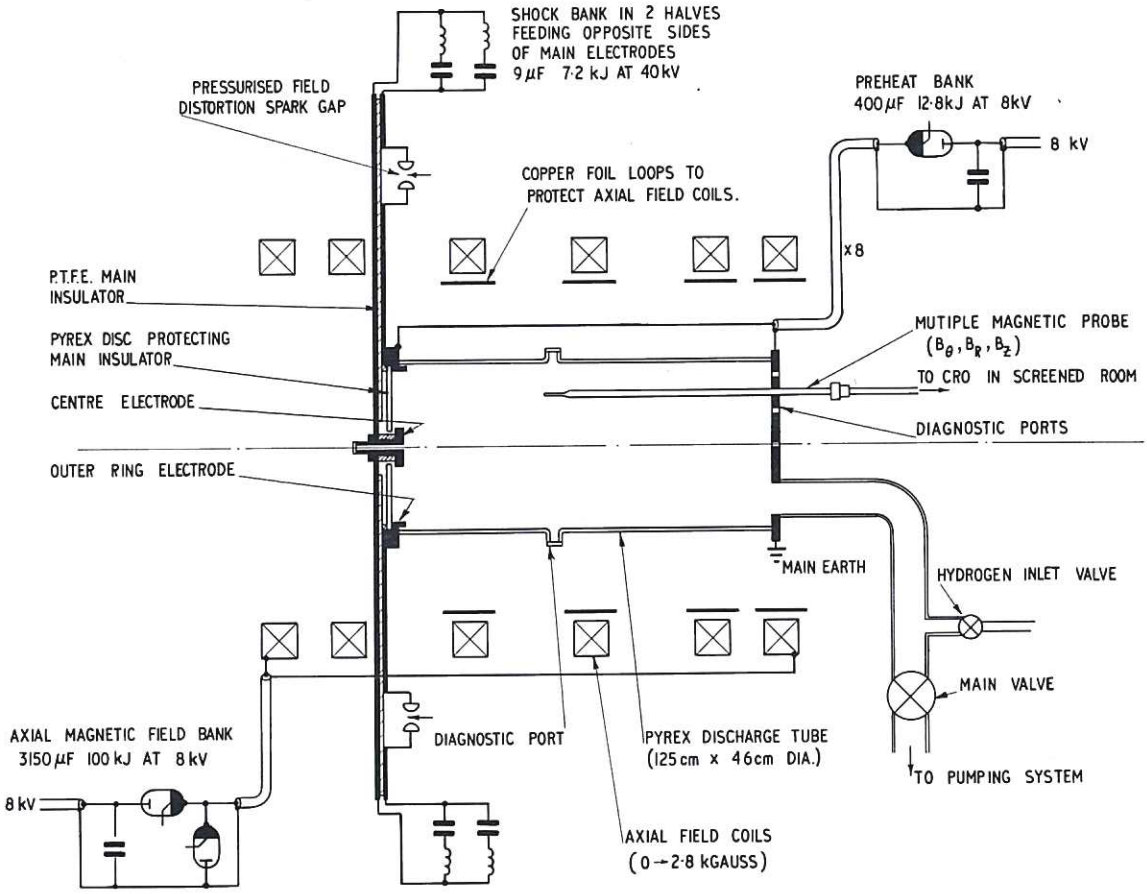

Fig.3 Schematic of the CHARYBDIS apparatus.

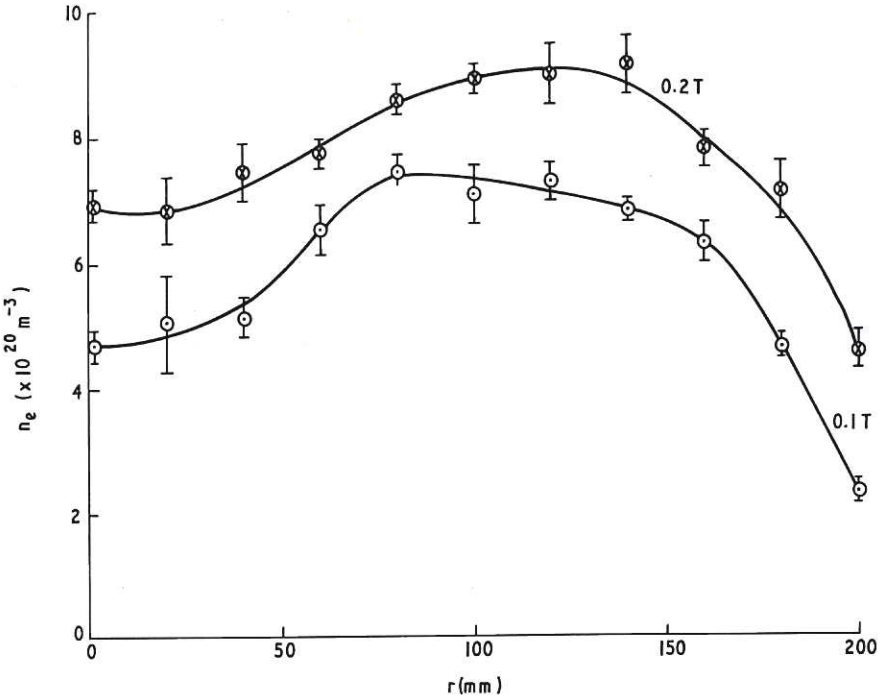

Fig.4 Radial density distribution of the initial plasma (z = 0.46 m, t = 300 μsec, p_1 = 20 mtorr, standard deviations of the mean).

CLM-P 318

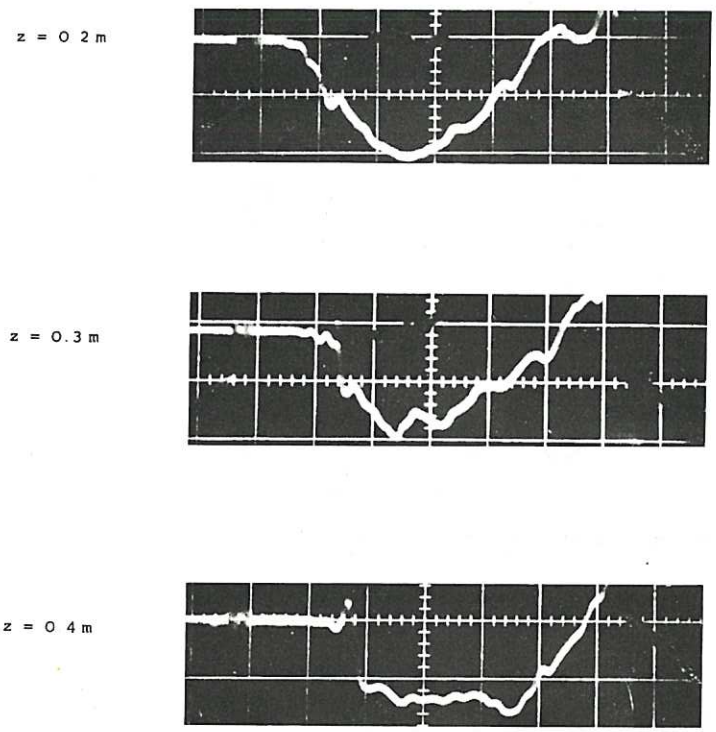

Fig.5 Propagation and steepening of the B_θ front (B_{z_1} = 0.1 T, r = 95 mm, 1 μsec/div, 0.13 T/div).

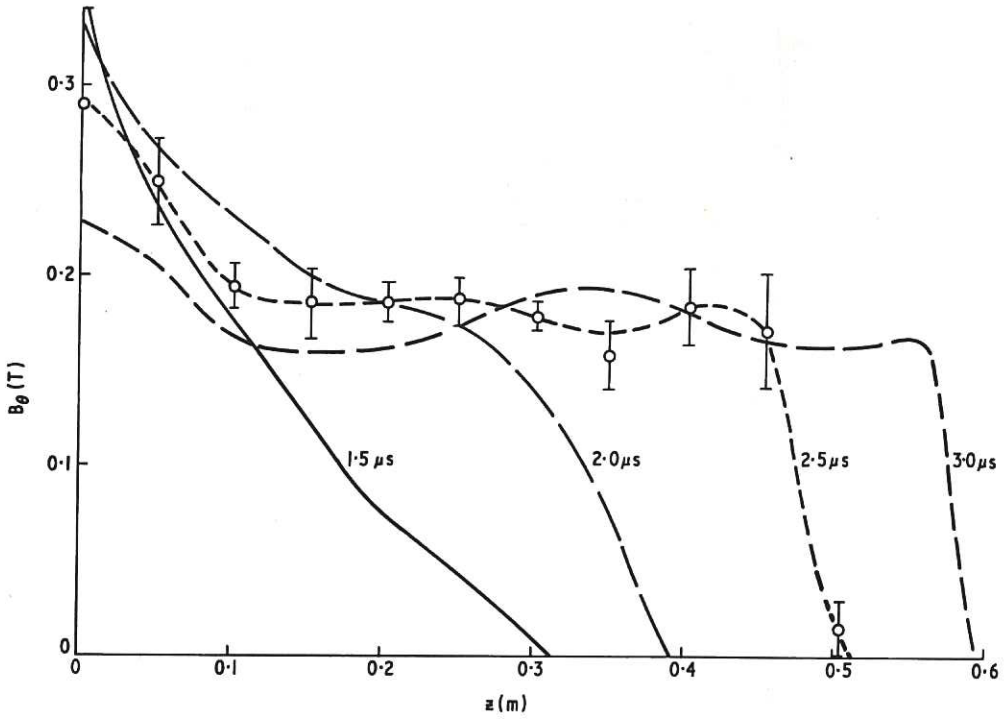

Fig.6 $B_\theta(z)$ profiles at successive times (B_{z_1} = 0.1 T, r = 95 mm, standard deviations).

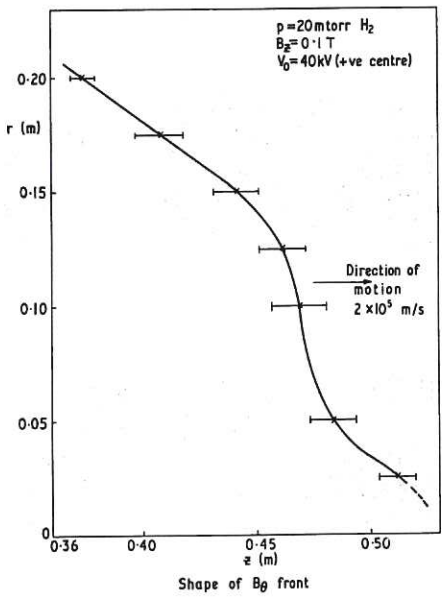

Fig.7 Shape of the B_θ front (B_{z_1} = 0.1 T, p_1 = 20 mtorr, standard deviations of the mean).

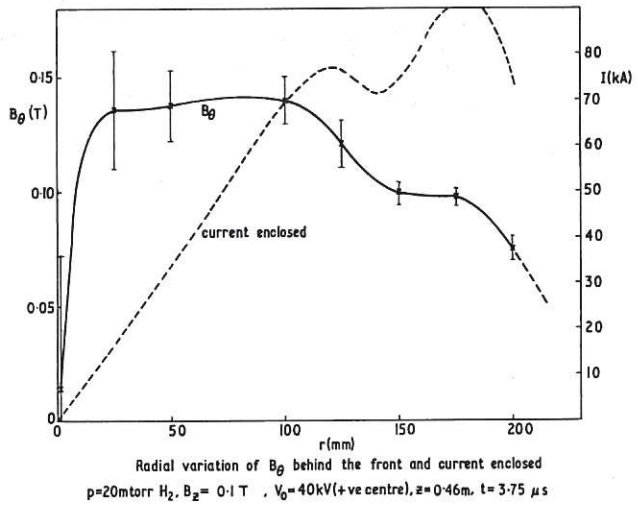

Fig.8 $B_\theta(r)$ and $I_z(r)$ profiles behind the B_θ front (B_{z_1} = 0.1 T, p_1 = 20 mtorr, standard deviations of the mean).

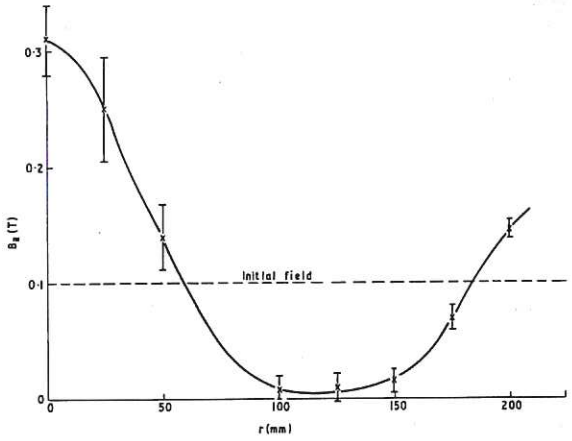

Fig.9 $B_z(r)$ profile behind the propagating front (B_{z_1} = 0.1 T, p_1 = 20 mtorr, standard deviations of the mean).

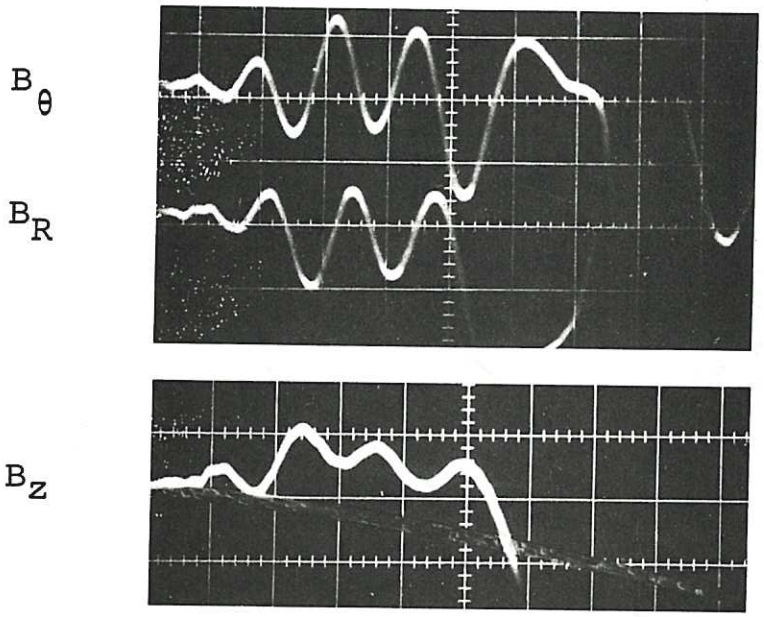

Fig.10 Precursor whistler oscillations (B_{z1} = 0.1 T, r = 95 mm, 0.2 μsec/div, 0.015 T/div).

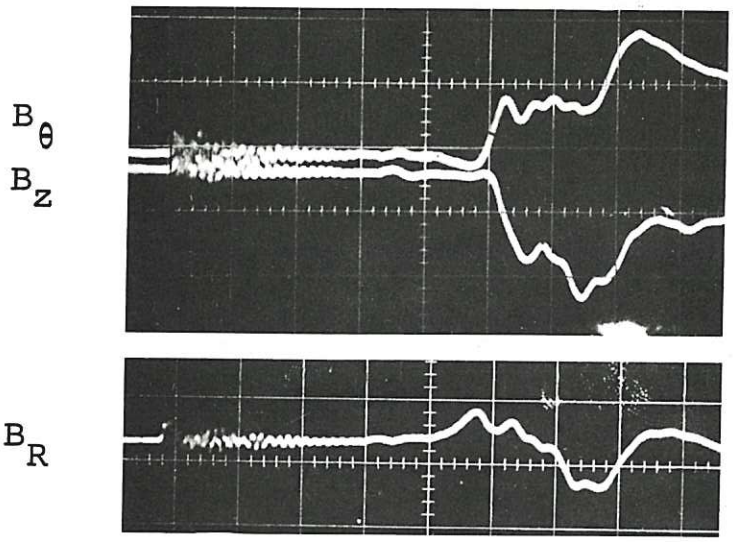

Fig.11 Typical oscillograms showing the magnetic structure of the front at low M_A (B_{z1} = 0.2 T, r = 50 mm, z = 0.6 m, 0.5 μsec/div, 0.14 T/div).

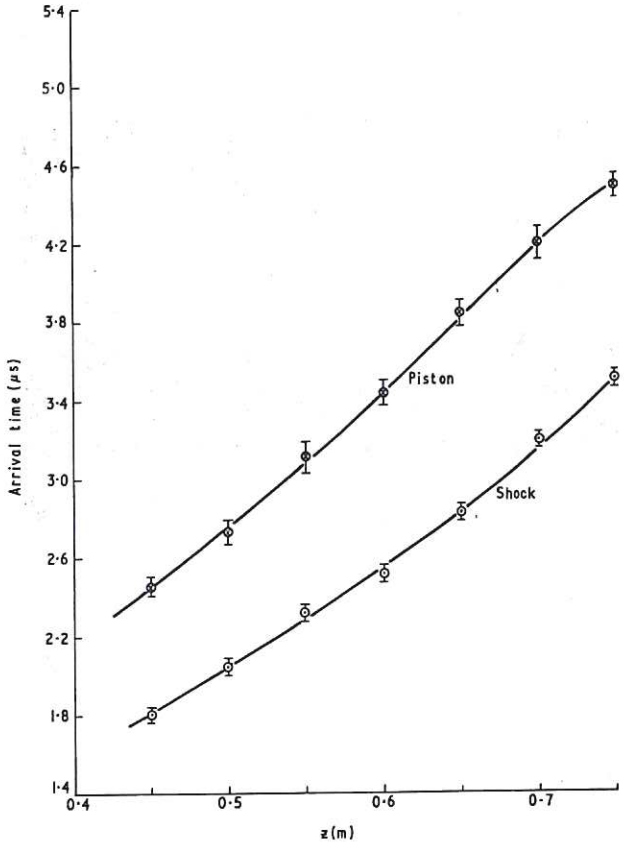

Fig.12 Axial propagation of the separate radial current fronts (B_{z1} = 0.2 T, r = 47.5 mm, standard deviations of the mean).

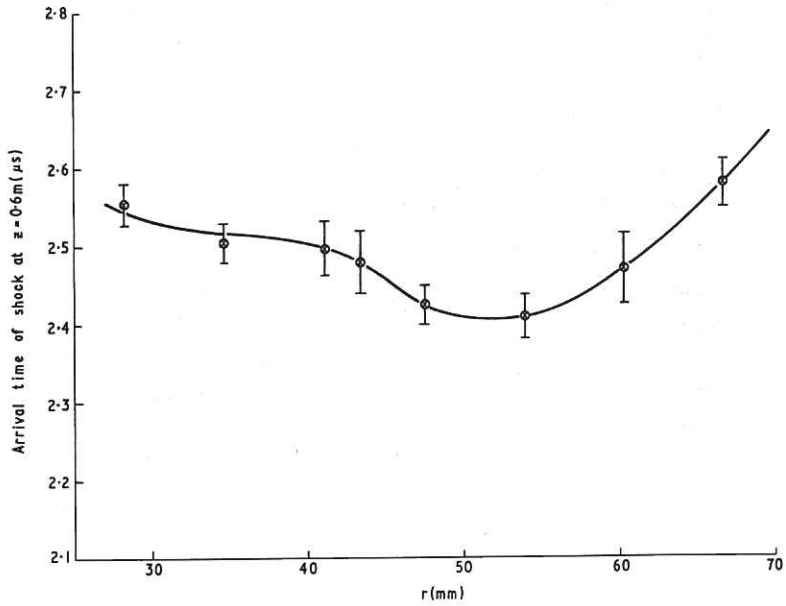

Fig.13 Radial variation in arrival time of the first radial current front (B_{z1} = 0.2 T, z = 0.6 m, standard deviations of the mean).

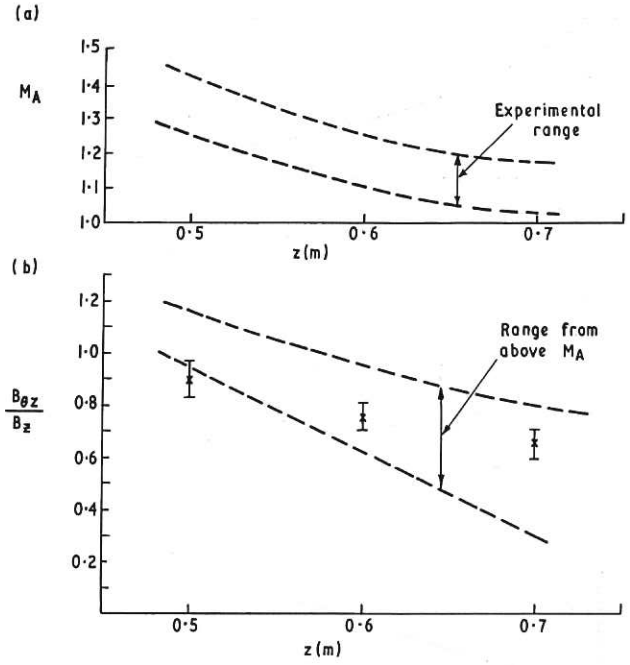

Fig.14 (a) Variation of experimental range of M_A with axial position. (b) Experimental and theoretical 'switched-on' field values (standard deviations of the mean).

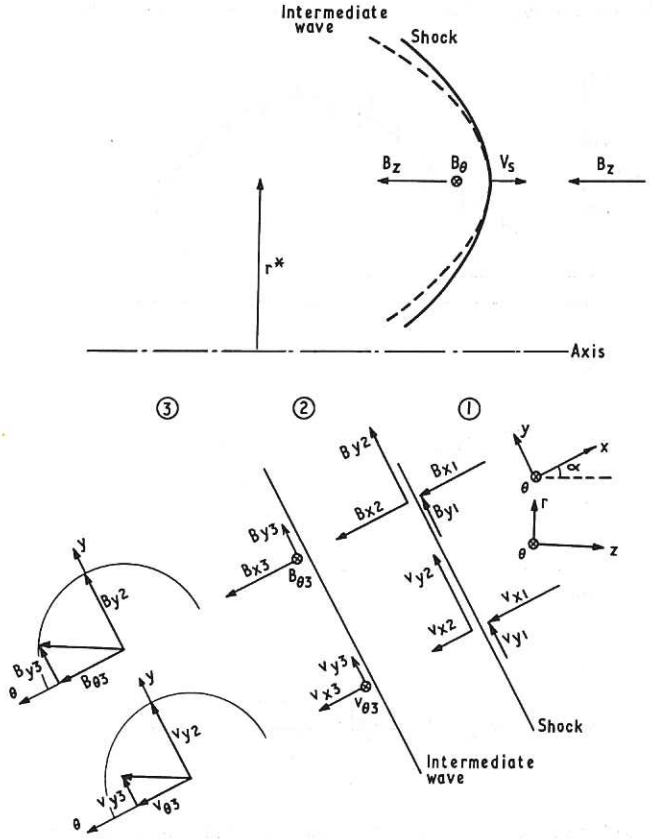

Fig.15 Shock-intermediate wave model.

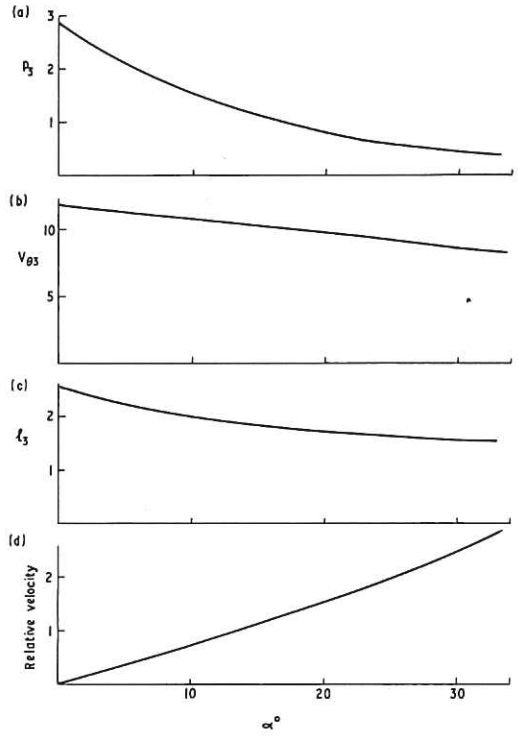

Fig.16 Theoretical (a) p_3 ($\times 10^3$ N/m^2), (b) v_{θ_3} ($\times 10^4$ m/sec), (c) ρ_3 ($\times 10^{-6}$ kg/m^3) and (d) relative velocity between shock and intermediate wave ($\times 10^4$ m/sec) plotted as functions of shock angle α ($B_{z_1} = 0.2$ T, $v_{A_1} = 15.4 \times 10^4$ m/sec. $M_A = 1.3$ at $\alpha = 0^o$).

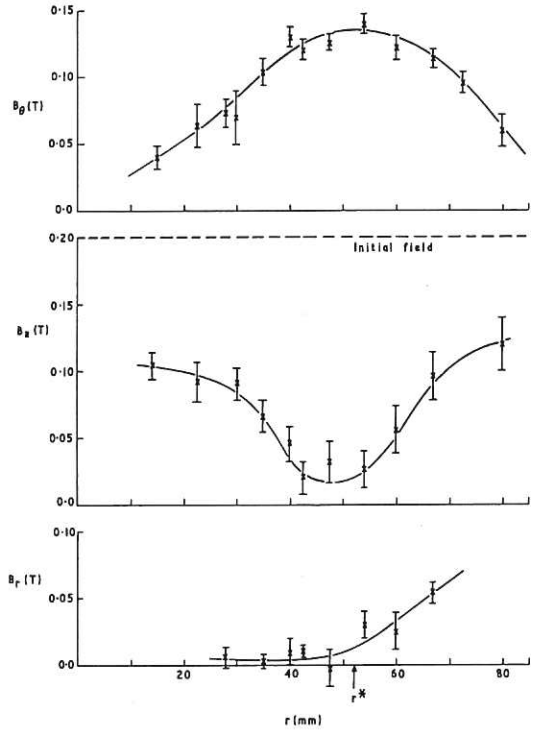

Fig.17 Radial variation of B_θ, B_z and B_R behind the shock/intermediate wave ($B_{z_1} = 0.2$ T, $z = 0.6$ m, standard deviations of the mean).

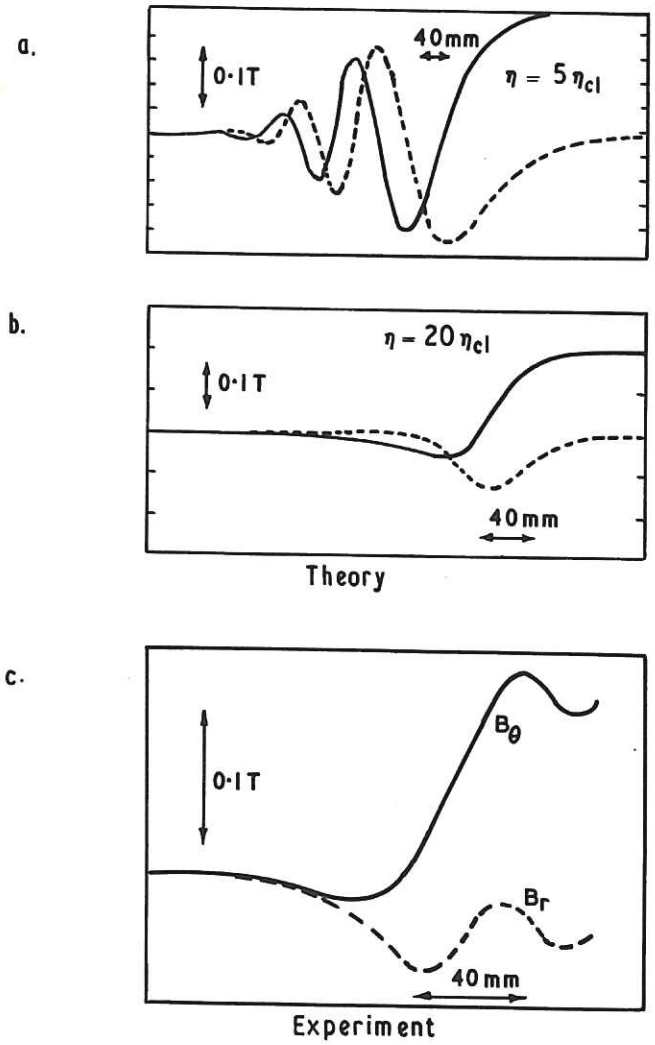

Fig.18 Comparison of computed and experimental switch-on shock structure ($M_A = 1.3$).

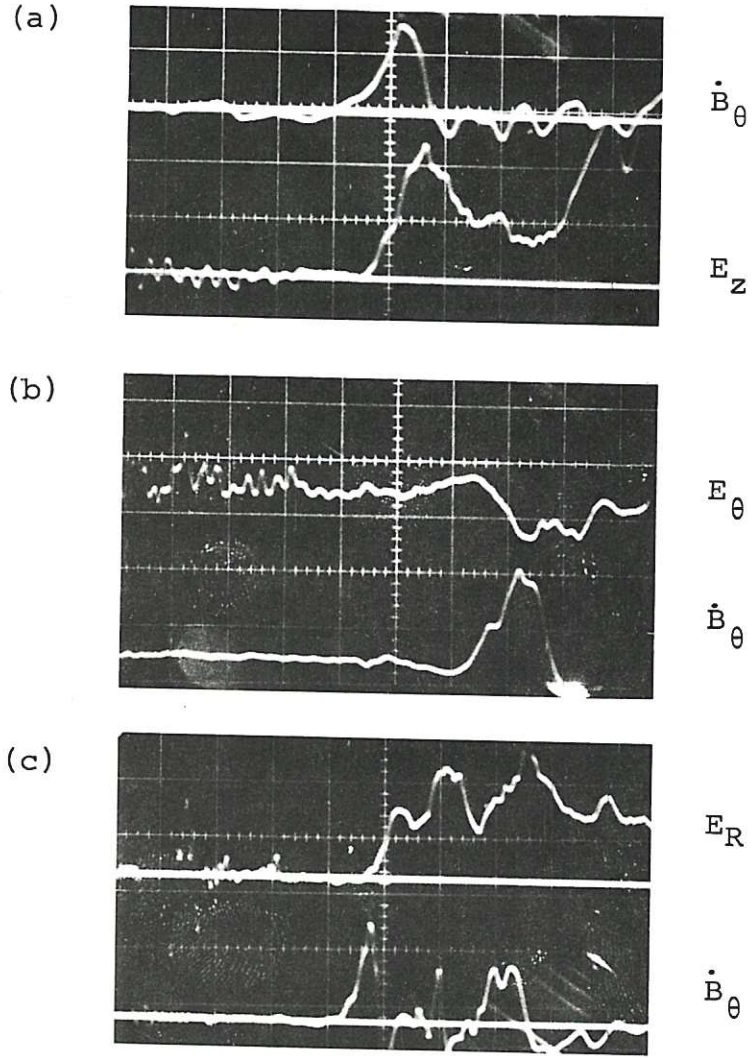

Fig.19 Typical oscillograms of electric field components; each is shown with the $\dot{B}_\theta$ signal of an adjacent magnetic probe. (r = 50 mm, z = 0.6 m, $\dot{B}_\theta$ 20 V/div, E_z 2×10^3 V/m/div, E_θ 5.7×10^3 V/m/div, 0.2 μsec/div, E_R 1.55×10^4 V/m/div 0.5 μsec/div).